Supplementary Materials for

Aerosol Induced Modification of Organised Convection and Top-of-Atmosphere Radiation

Nidhi Nishant[1,2,3], Steven C. Sherwood[1,2], Olivier Geoffroy[1,4]

[1] Climate Change Research Centre, [2]ARC Centre of Excellence for Climate System Science, University of New South Wales, Sydney, New South Wales, Australia, [3]NSW Department of Planning, Industry and Environment, Sydney, Australia, [4] National Centre for Meteorological Research, France

Corresponding author: Nidhi Nishant (n.nidhi@unsw.edu.au)

This file includes:

Supplementary Text
Supplementary Figures 1 to10
Supplementary Tables 1 to 4
References

Supplementary Text

Additional results from the WRF simulations

Supplementary Figure 2 shows the frequency distribution of updraft velocities in the convective zone (i.e. Equator to 5 °latitude) and between 6-11 km altitude. The updrafts become stronger in both PERT2 and POLL2 experiments in comparison to Control2 in all the 2-km experiments irrespective of the physics options selected (Supplementary Table 5) suggesting extra buoyant updrafts possibly invigorating the convective clouds (Supplementary Figure 2 a,c,e). PERT20 experiments (Supplementary Figure 2 b,d,f) also show a similar signal, however the updraft velocities are weaker in comparison to the POLL2 and PERT2 experiments. Thus, all the experiments show clear sign of invigoration.

The strengthening of updrafts is followed by broadening of the clouds (Supplementary Figure 3). Similar changes in the cloud fraction are seen in all nine experiments. The clouds spread to higher latitudes and there is an overall increase in the cloud fraction of the mid and high-level clouds (Supplementary Table 4), however at the Equator, concentration and enhancement of rain (Supplementary Figure 6) desiccates the cloud thus reducing the cloud fraction. Note that changes to the cirrus layer and clouds near the surface vary depending on the experiment design and are not considered robust.

PERT20c experiment shows strong reduction in the shallow clouds (Supplementary Figure 3 c), which can be attributed to convective scheme. We use the Betts-Miller cumulus parameterization (1), which is an adjustment type scheme. Based on the availability of the convective potential energy (CAPE), this scheme either triggers the deep convection or the shallow convection. When the latent heating perturbations are added between 6-8 km altitude, it decreases the CAPE. This shifts the deep convection to shallow convection and the enhanced shallow convection reduces the low cloud amount. As Control20a and Control20b simulations (Supplementary Figure 3 f,i) fail to simulate enough shallow clouds there is negligible changes in shallow cloud in these simulations. However, PERT2b and POLL2b simulations show slight enhancement in the shallow clouds.

Vertically averaged spatial profiles of cloud fraction and precipitation show similar broadening of clouds and narrowing of deep convective region rain band in all the experiments (Supplementary Figs. 4 and 5) except for the two experiments i.e. PERT20a and PERT20b (Supplementary Figure 5 b,d) which fail to report the narrowing of the deep convective region rain-band. Past studies have suggested that factors like mass flux largely controls the convective cloud amount, however, except PERT2a none of the perturbed experiments show an increase in the mass flux (Supplementary Figure 6).

The perturbed experiments show a warmer atmosphere (on an average by 0.5^{o} C between 6 and 12 km altitude) in comparison to the control experiments (Figure 3), due to warmer updrafts enhancing upward heat transport. In addition to warming at the higher altitudes, there is also seen warming of the lower troposphere (Supplementary Figure 7). This warming is associated with the strengthening of the shallow circulations which via transport of static energy warms the lower atmosphere.

Regression Model	r^2		Number of boxes Positive/Negative		AOD Coefficient		r^2 Train/Test	
	Tropics	**Midlatitudes**	**Tropics**	**Midlatitudes**	**Tropics**	**Midlatitudes**	**Tropics**	**Midlatitudes**
AOD	**0.09**	**0.12**	**212/388**	**40/297**	**-0.04**	**-0.21**	**0.12/0.10**	**0.14/0.12**
AOD + RH	**0.25**	**0.27**	**166/434**	**47/290**	**-0.06**	**-0.25**	**0.28/0.22**	**0.30/0.22**
AOD +UA	**0.16**	**0.18**	**185/415**	**43/294**	**-0.05**	**-0.22**	**0.19/0.16**	**0.20/0.16**
AOD + VA	**0.16**	**0.16**	**208/392**	**38/299**	**-0.05**	**-0.24**	**0.21/0.19**	**0.20/0.18**
AOD + P_Area	**0.17**	**0.18**	**217/383**	**41/296**	**-0.06**	**-0.26**	**0.21/0.21**	**0.19/0.17**
AOD + UA + VA	**0.21**	**0.21**	**223/377**	**115/222**	**-0.02**	**-0.13**	**0.24/0.16**	**0.26/0.13**
AOD + RH + UA + VA	**0.31**	**0.25**	**254/346**	**119/218**	**-0.02**	**-0.11**	**0.37/0.21**	**0.29/0.11**
AOD + RH + UA + VA + P_Area	**0.34**	**0.31**	**267/333**	**160/177**	**-0.03**	**-0.07**	**0.41/0.22**	**0.30/0.11**

Supplementary Table 1: List of regression models to predict the changes in area ratios using AOD, RH, UA, VA data from CAMS and area ratio and P_Area data from the TRMM database. Here, column 2 and 3 shows r^2 which denotes the coefficient of multiple regression, column 4 and 5 shows the number of boxes where the coefficient of AOD is positive and/ negative, whereas column 6 and 7 shows the median coefficient of AOD for Tropics and Midlatitudes regions respectively. Column 8 and 9 denotes the r^2 for the train and test dataset for Tropics and Midlatitudes regions respectively. Models in italics are found to overfit the results.

Regression Model	r^2		Number of boxes Positive/Negative		AI Coefficient		r^2 Train/Test	
	Tropics	**Midlatitudes**	**Tropics**	**Midlatitudes**	**Tropics**	**Midlatitudes**	**Tropics**	**Midlatitudes**
AI_{CAMS}	**0.08**	**0.10**	**223/379**	**64/279**	**-0.03**	**-0.26**	**0.10/0.09**	**0.12/0.10**
AI_{CAMS} + RH	**0.24**	**0.19**	**149/451**	**45/292**	**-0.12**	**-0.29**	**0.28/0.23**	**0.22/0.20**
AI_{CAMS} +UA	**0.17**	**0.20**	**218/382**	**51/286**	**-0.02**	**-0.28**	**0.21/0.19**	**0.23/0.21**
AI_{CAMS} + VA	**0.16**	**0.16**	**238/362**	**46/291**	**-0.01**	**-0.29**	**0.20/0.18**	**0.17/0.14**
AI_{CAMS} + P_Area	**0.16**	**0.14**	**229/371**	**58/279**	**-0.02**	**-0.27**	**0.21/0.20**	**0.20/0.20**
AI_{CAMS} + UA + VA	**0.22**	**0.23**	**234/366**	**88/249**	**-0.03**	**-0.15**	**0.27/0.18**	**0.30/0.19**
AI_{CAMS} + RH + UA + VA	**0.31**	**0.28**	**252/238**	**89/248**	**-0.01**	**-0.04**	**0.37/0.12**	**0.34/17**
AI_{CAMS} + RH + UA + VA + P_Area	**0.34**	**0.31**	**267/333**	**145/192**	**-0.02**	**-0.01**	**0.30/0.11**	**0.34/0.14**

Supplementary Table 2. Same as Table S1 but using AI_{CAMS} in place of AOD from CAMS.

Regression Model	r^2		Number of boxes Positive/Negative		AI Coefficient		r^2 Train/Test	
	Tropics	**Midlatitudes**	**Tropics**	**Midlatitudes**	**Tropics**	**Midlatitudes**	**Tropics**	**Midlatitudes**
AI_{TOMS}	**0.09**	**0.10**	**196/404**	**120/217**	**-0.06**	**-0.06**	**0.10/0.7**	**0.09/0.07**
AI_{TOMS} + RH	**0.23**	**0.13**	**247/353**	**117/220**	**-0.07**	**-0.08**	**0.29/0.24**	**0.13/0.11**
AI_{TOMS} +UA	**0.15**	**0.14**	**212/388**	**131/206**	**-0.07**	**-0.03**	**0.18/0.13**	**0.20/0.18**
AI_{TOMS} + VA	**0.16**	**0.12**	**214/386**	**120/217**	**-0.06**	**-0.05**	**0.19/0/16**	**0.20/0.16**
AI_{TOMS} + P_Area	**0.15**	**0.15**	**199/401**	**103/234**	**-0.07**	**-0.08**	**0.19/0.17**	**0.20/0.19**
AI_{TOMS} + UA + VA	**0.21**	**0.18**	**222/378**	**89/248**	**-0.02**	**-0.05**	**0.26/0.18**	**0.21/0.16**
AI $_{TOMS}$+ RH + UA + VA	**0.30**	**0.23**	**242/358**	**95/242**	**-0.02**	**-0.04**	**0.36/0.08**	**0.34/0.21**
AI_{TOMS} + RH + UA + VA + P_Area	**0.33**	**0.28**	**273/327**	**149/188**	**-0.04**	**-0.01**	**0.40/0.18**	**0.36/0.17**

Supplementary Table 3: Same as Table S1 but using AI_{TOMS} in place of AOD from CAMS.

Variables	POLL2a	POLL2b	POLL2c	PERT2a	PERT2b	PERT2c	PERT20a	PERT20b	PERT20c
Cloud Fraction (%)	**0.45**	**1.22**	**1.20**	**0.80**	**1.31**	**1.13**	**0.24**	**0.68**	**0.87**
Latent Heating (K/day)	**0.10**	**0.49**	**0.17**	**0.55**	**0.91**	**0.71**	**0.10**	**0.21**	**0.30**
Updraft velocity w (m/s)	**0.57**	**0.10**	**0.27**	**0.15**	**0.16**	**0.11**	**0.18**	**0.21**	**0.19**
Temperature T (K)	**0.13**	**0.36**	**0.47**	**0.24**	**1.49**	**0.60**	**0.30**	**0.48**	**0.37**
Cloud Radiative Effect (W/m^2)	**-1.84**	**-1.88**	**-1.05**	**-1.22**	**-2.47**	**-2.8**	**-2.28**	**-2.20**	**-3.50**
Precipitation (mm/day)	**-18**	**-10**	**-73**	**-15**	**-16**	**-212**	**21**	**16**	**-11**
Mass Flux (Kg/m^2 s)	**-0.01**	**-0.18**	**-0.08**	**0.01**	**-0.15**	**-0.02**	**-0.01**	**-0.03**	**-0.01**

Supplementary Table 4. Differences of variables between the perturbed and control experiments, averaged from 0-10^o latitude. Cloud fraction, latent heating, updraft speed, updraft mass flux and temperature are averaged between 6-12 km altitude. Cloud radiative effect is calculated at the top of the atmosphere and is an average between 0-15^o latitude.

We also performed a suite of experiments to test the stabilisation-stratification hypothesis by running short experiments (24 hours duration) by restarting the model. These experiments are done by restarting the CONTROL20 and CONTROL2 experiment on a fixed day and are run for a period of 24 hours. Experiments are performed in which we, to investigate how the lifetime and amount of clouds respond. In two runs the model is restarted with a dry boundary layer to prevent development of further convection; in one (DBL) this is the only change, while in the other (DBLW), the lapse rate is also decreased by 0.04 K/km between surface and 14 km altitude. Three sets of such experiments are performed at 20 km resolution by initializing the model on its 70th, 80th and 90th day whereas one set of experiment is performed at 2 km resolution (70th day) to test the robustness of the results. Names of these experiments are followed by suffix 20 and 2 for resolution and a, b and c for the initialization day respectively.

With the drying of the boundary layer all the experiments show a suppression in precipitation (Supplementary Figure 10). Additionally, the stabilised experiment (DBLW) show increased cloud fraction relative to unstabilised DBL (Supplementary Figure 8 b,d,f). It can be noted that the impact of the lapse rate change was robust across all three ensemble members supporting our hypothesis that stabilisation of the atmosphere is responsible for enhancing the cloud fraction throughout most of the troposphere.

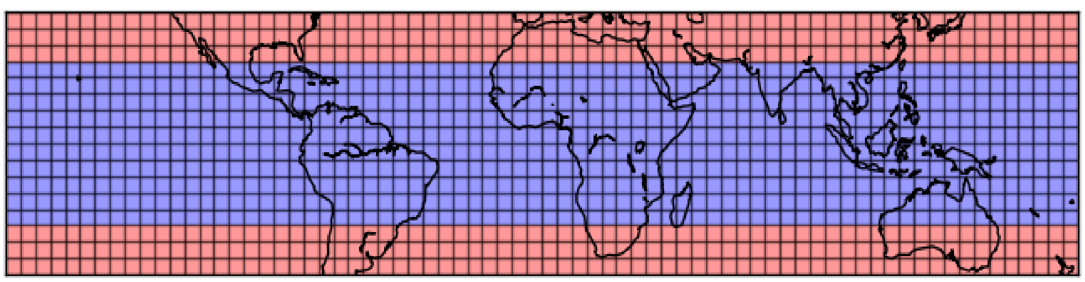

Supplementary Figure 1: Locations of the 1152 square boxes selected in the Tropics and mid-latitudes. Boxes marked in blue and red colour denote Tropical and mid-latitudinal boxes respectively

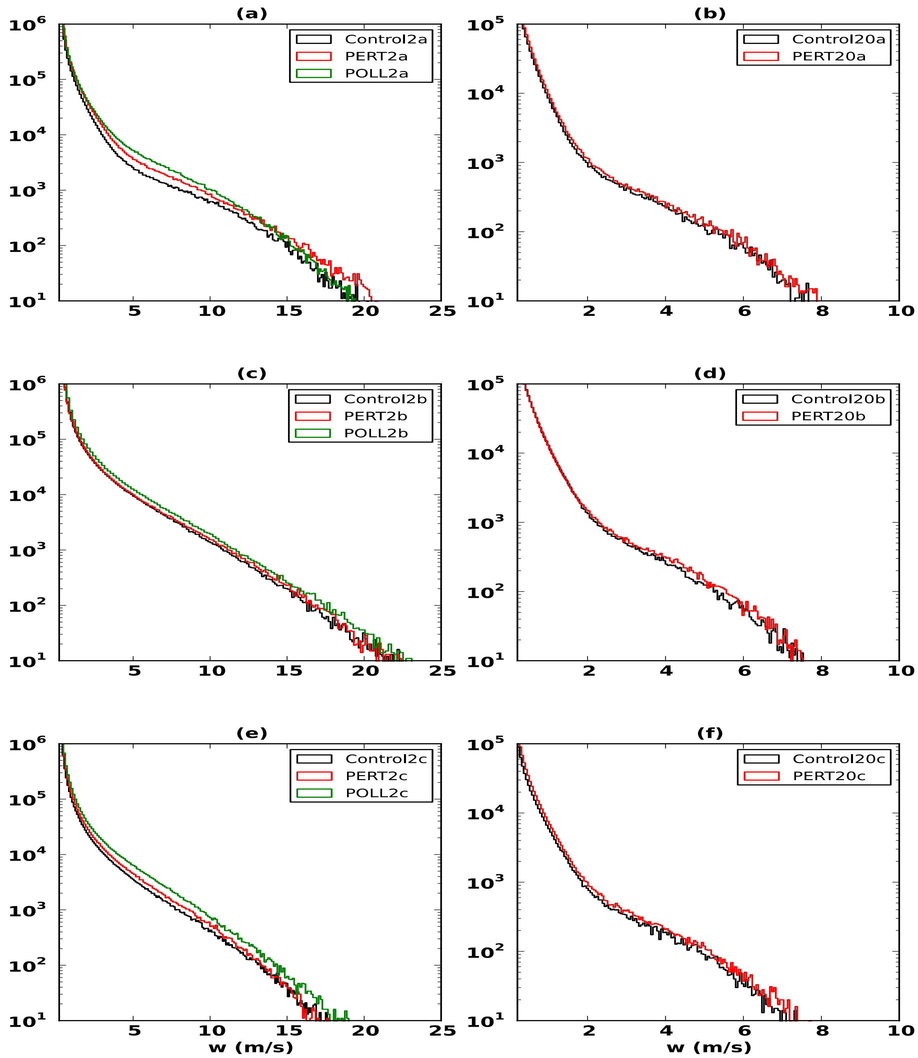

Supplementary Figure 2. Frequency distribution of updrafts in the convective zone i.e. between Equator to 5 ° latitude and 6-11 km altitude. Here black, red and green colors represent Control, PERT and POLL experiments respectively, whereas (a,c,e) and (b,d,f) represent 2 km and 20 km resolution experiments respectively. First (a,b), second (c,d) and third (e,f) row represents experiments with Morr2-RRTM, WDM6-RRTM and WDM6-Dudhia physics respectively.

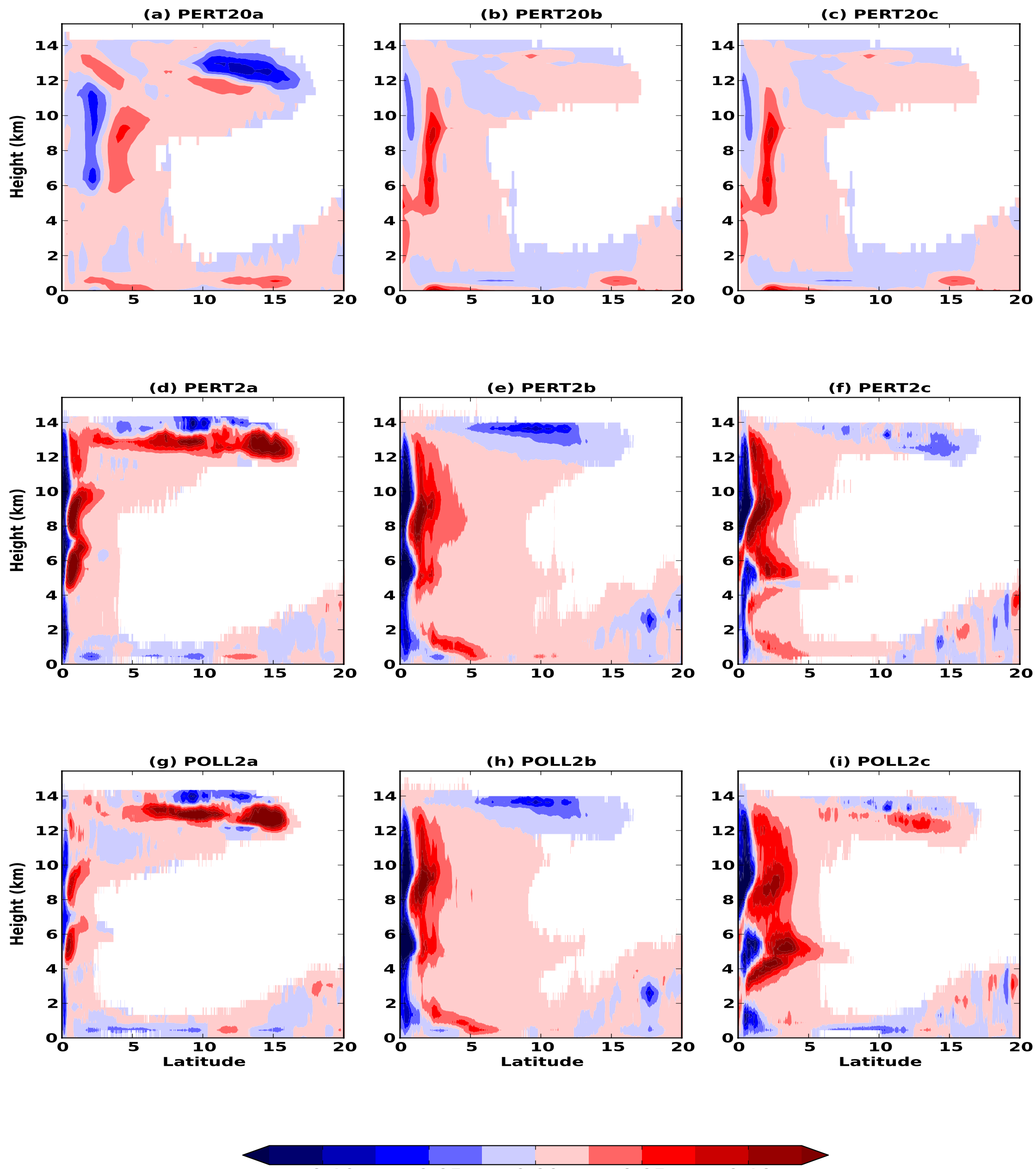

Supplementary Figure 3. Impact of aerosols on simulated cloud amount. Zonal and temporal averages of difference in cloud fraction between PERT20a and Control20a (a), PERT20b and Control20b (b), PERT20c and Control20c (c), PERT2a and Control2a (d), PERT2b and Control2b (e), PERT2c and Control2c (f), POLL2a and Control2a (g), POLL2b and Control2b (h), and POLL2c and Control2c (i).

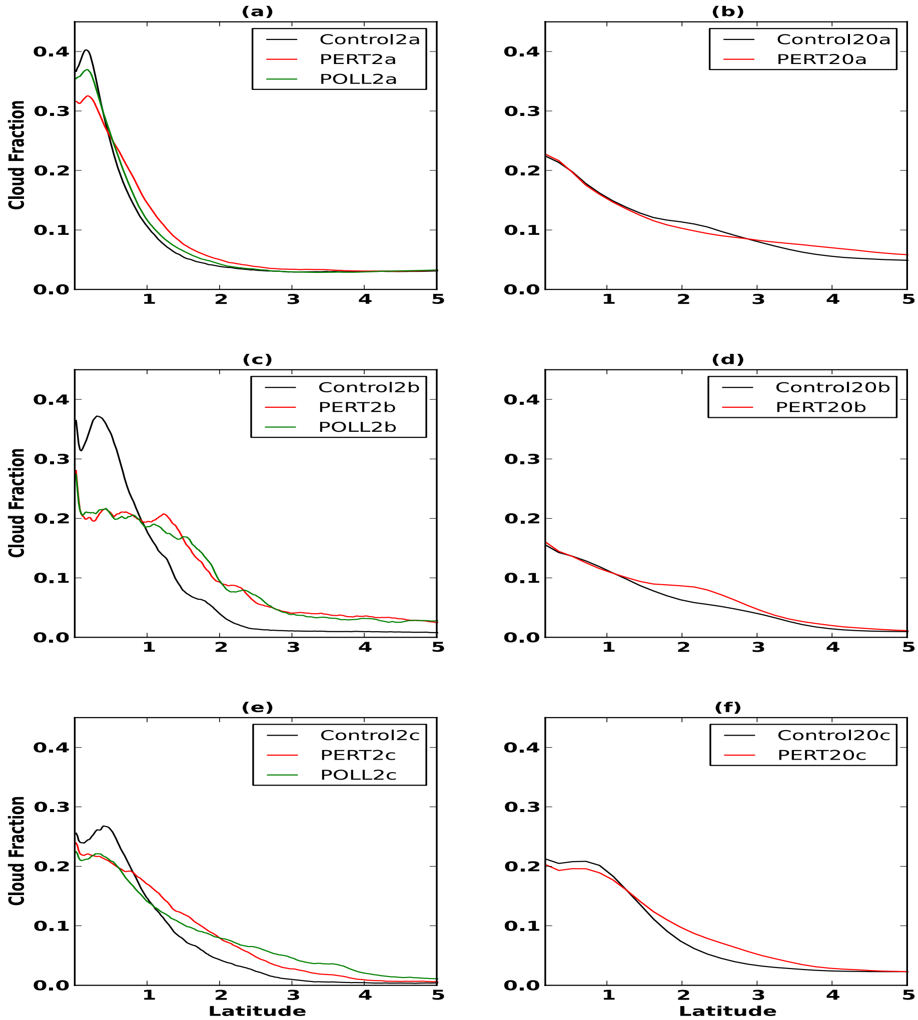

Supplementary Figure 4. Impact of aerosols on simulated zonal-mean total cloud. Zonally, temporally and vertically (between 6-11 km) averaged spatial profiles of cloud fraction for the 2-km (a,c,e) and 20-km (b,d,f) resolution experiments. Here black, red and green colors represent Control, PERT and POLL experiments respectively and first (a,b), second (c,d) and third (e,f) row represents experiments with Morr2-RRTM, WDM6-RRTM and WDM6-Dudhia physics respectively.

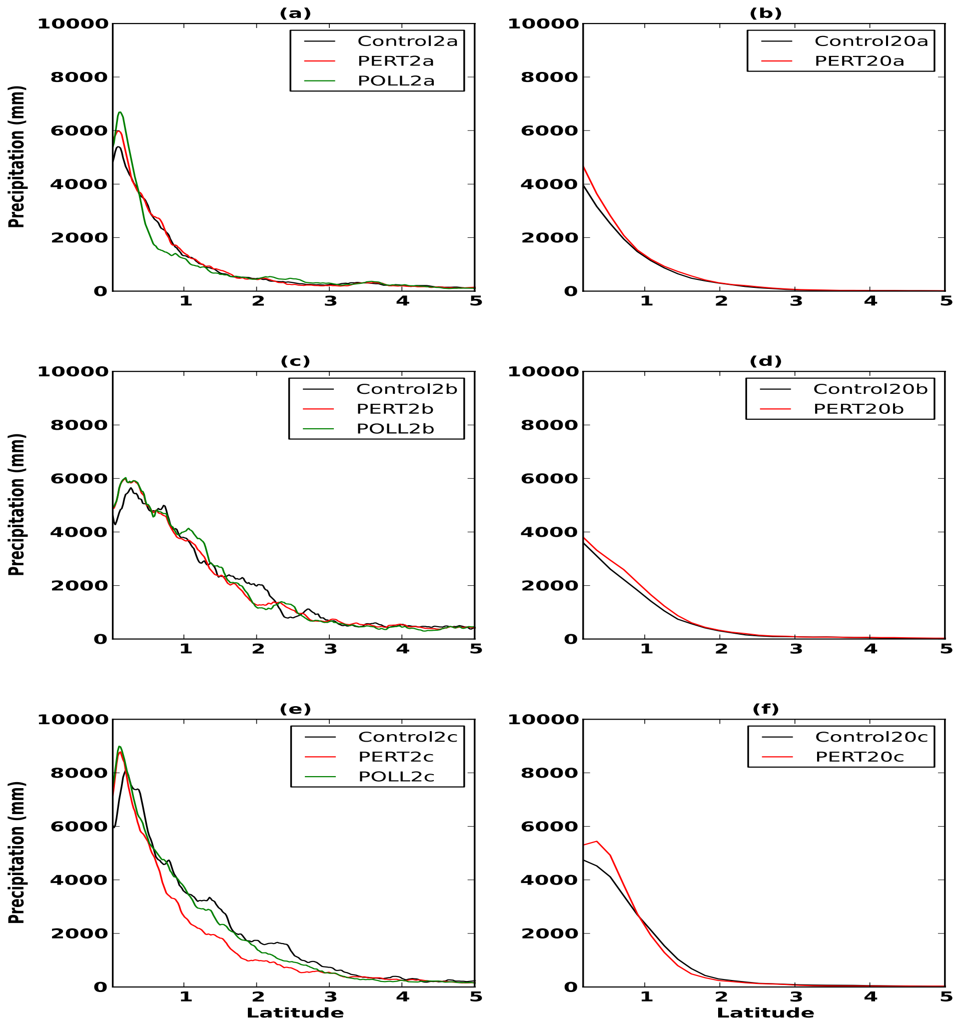

Supplementary Figure 5. Impact of aerosols on simulated zonal-mean precipitation. Zonally and temporally averaged spatial profiles of precipitation for the 2-km (a,c,e) and 20-km (b,d,f) resolution experiments. Here black, red and green colors represent Control, PERT and POLL experiments respectively and first (a,b), second (c,d) and third (e,f) row represents experiments with Morr2-RRTM, WDM6-RRTM and WDM6-Dudhia physics respectively.

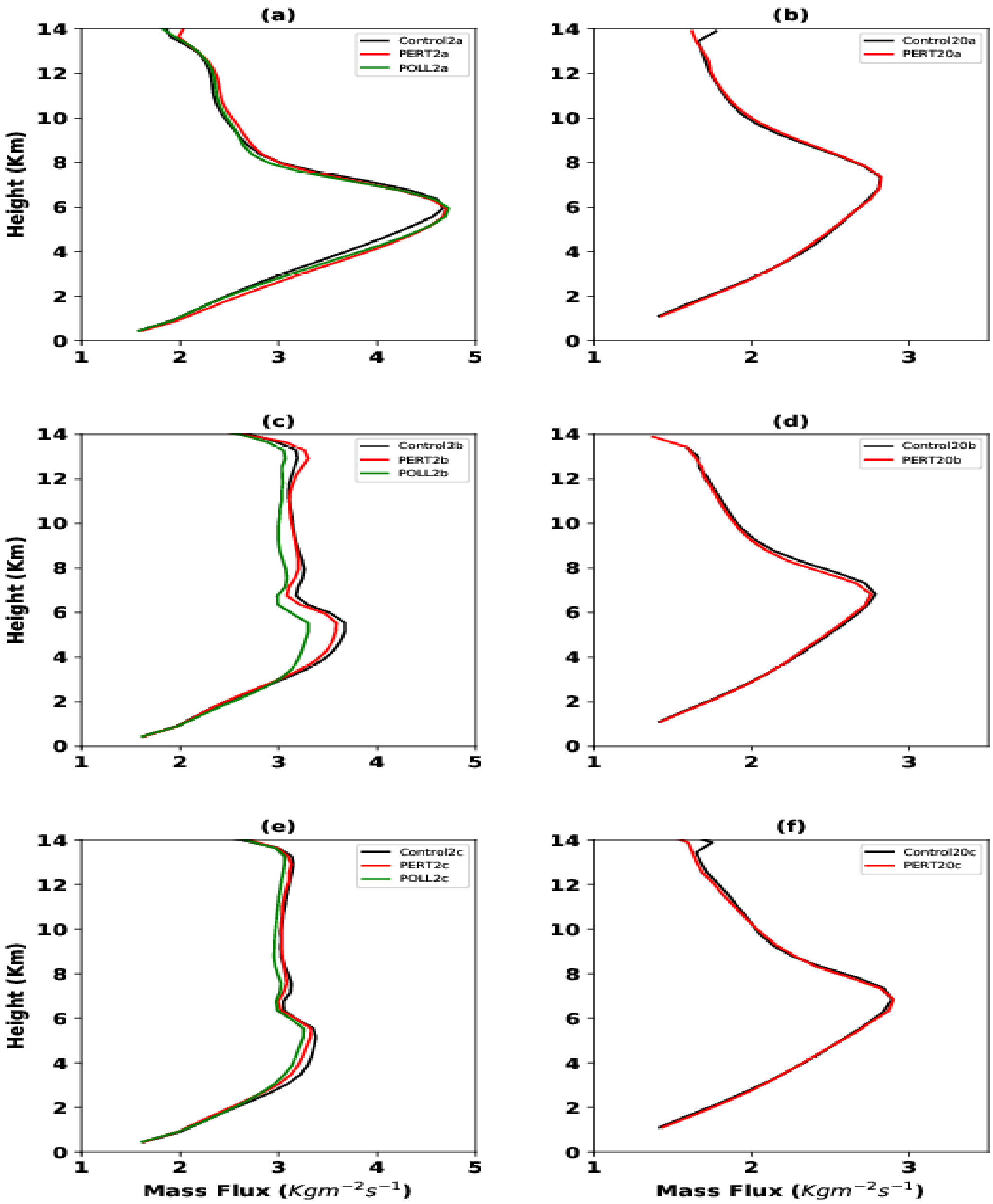

Supplementary Figure 6: Spatially and temporally averaged vertical profiles of mass flux for the 2-km (a,c,e) and 20-km (b,d,f) resolution experiments. Here black, red and green colors represent Control, PERT and POLL experiments respectively, whereas (a,c,e) and (b,d,f) represent 2 km and 20 km resolutions respectively. First (a,b), second (c,d) and third (e,f) rows represent the (Morr2-RRTM), (WDM6-RRTM), and (WDM6-Dudhia) experiments respectively.

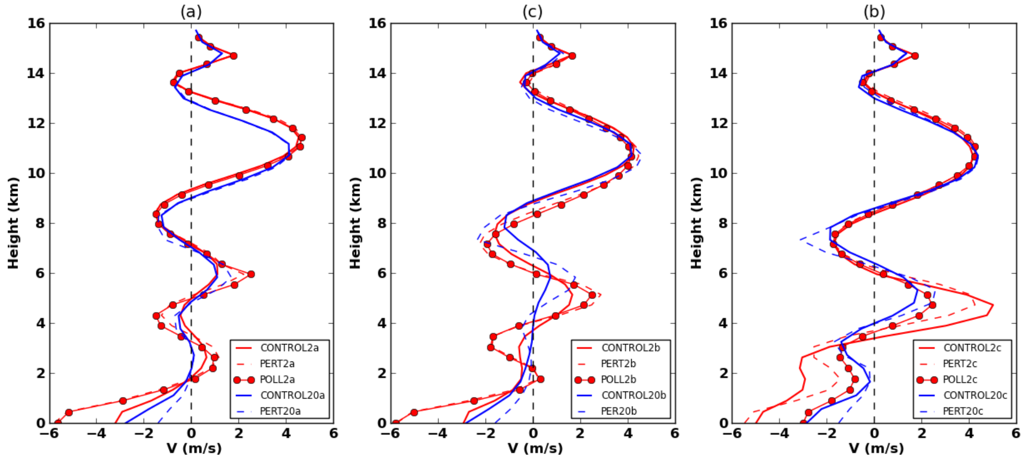

Supplementary Figure 7 Vertical profile of mean meridional wind in the ascending region, i.e. between Equator to 10 latitude of the simulation. Here, subplots (a), (b) and (c) denote the Morr2- RRTM, WDM6-RRTM and WDM6-Dudhia physics respectively.

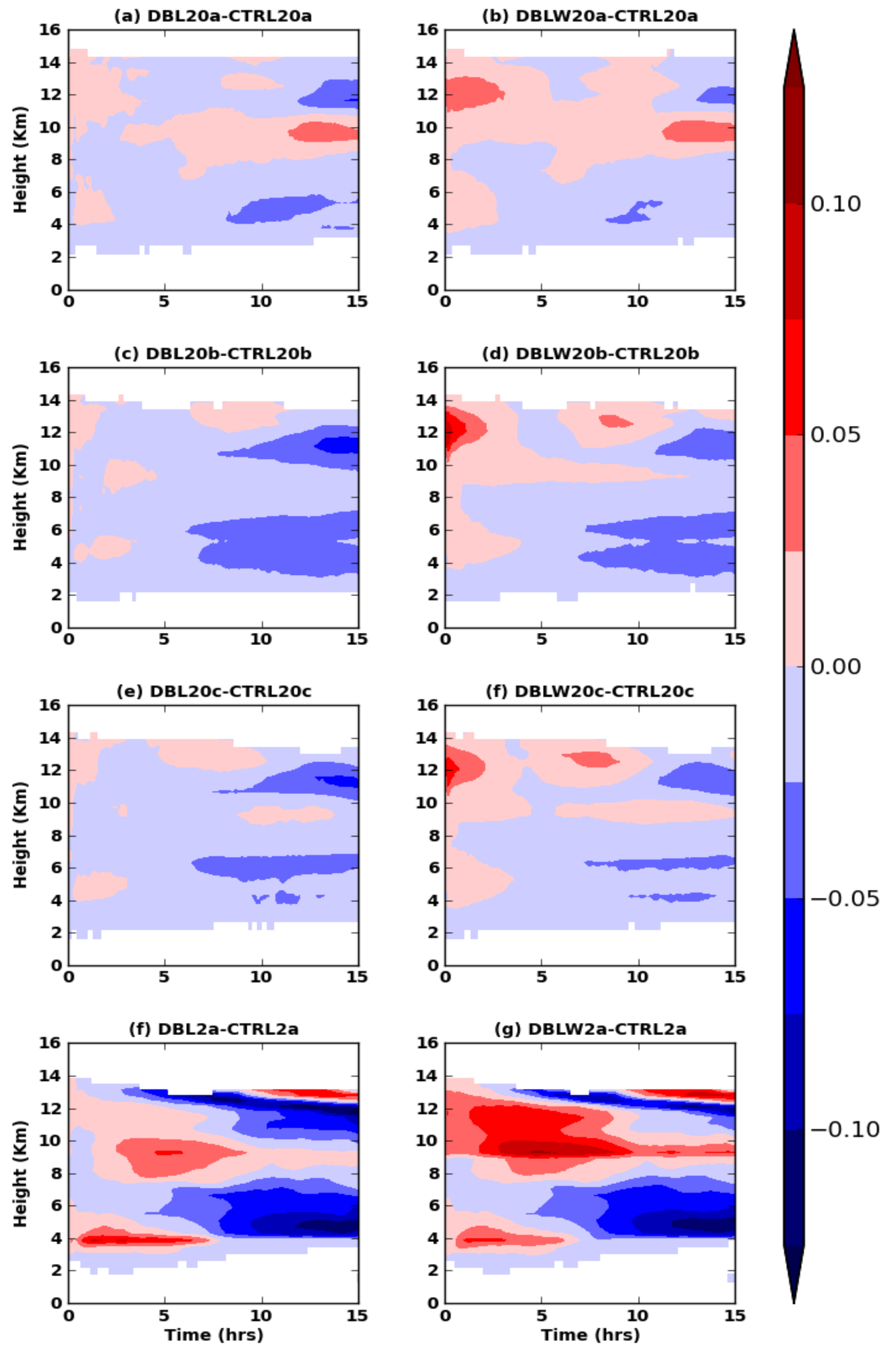

Supplementary Figure 8 Timeseries of vertical profiles of difference in cloud fraction between (a,c,e,f) DBL and CTRL and (b,d,f,g) DBLW and CTRL for three sets of experiment a, b and c at 20 km resolution and one set of experiment a at 2 km resolution.

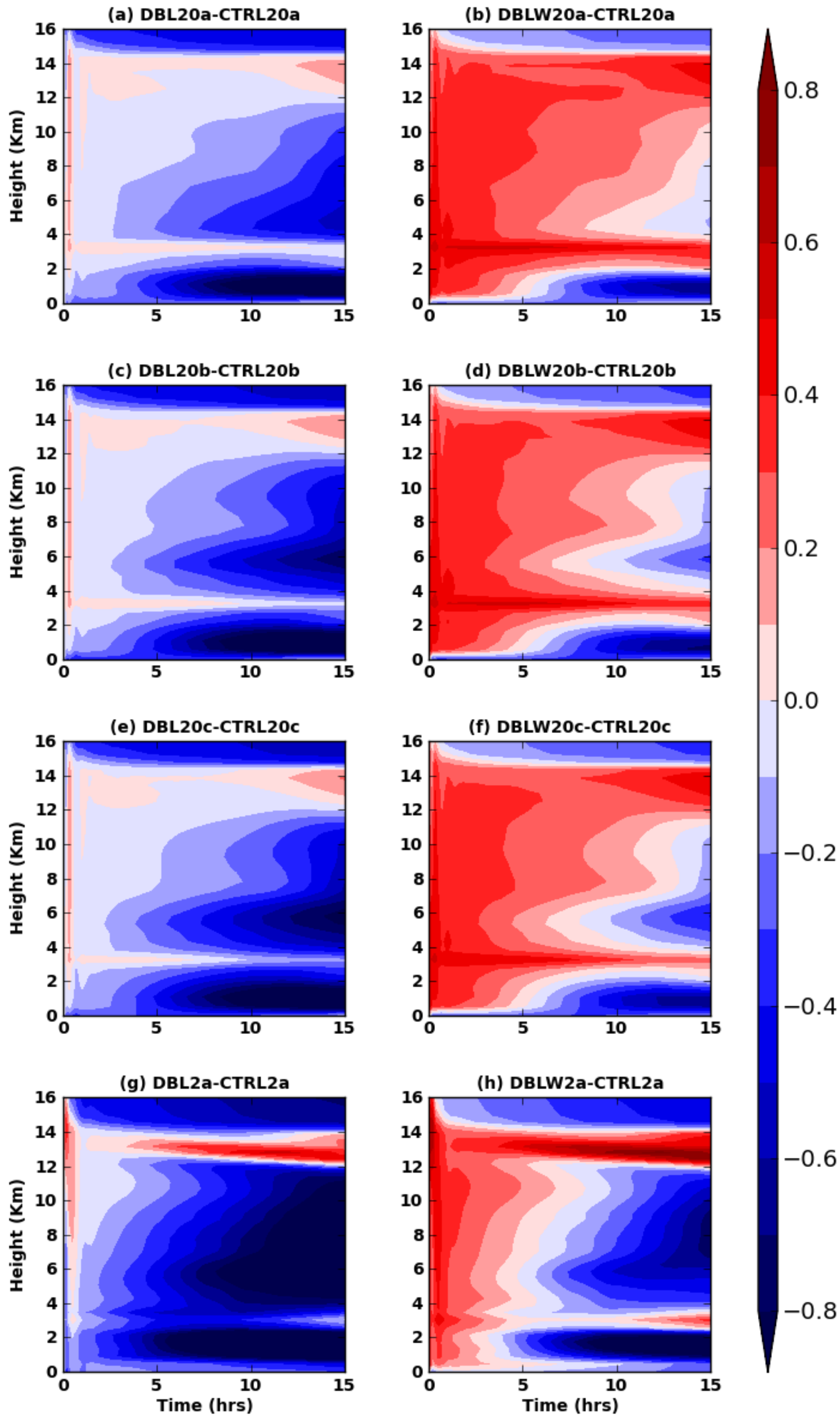

Supplementary Figure 9 Timeseries of vertical profiles of difference in temperature between (a,c,e,f) DBL and CTRL and (b,d,f,g) DBLW and CTRL for three sets of experiment a, b and c at 20 km resolution and one set of experiment a at 2 km resolution.

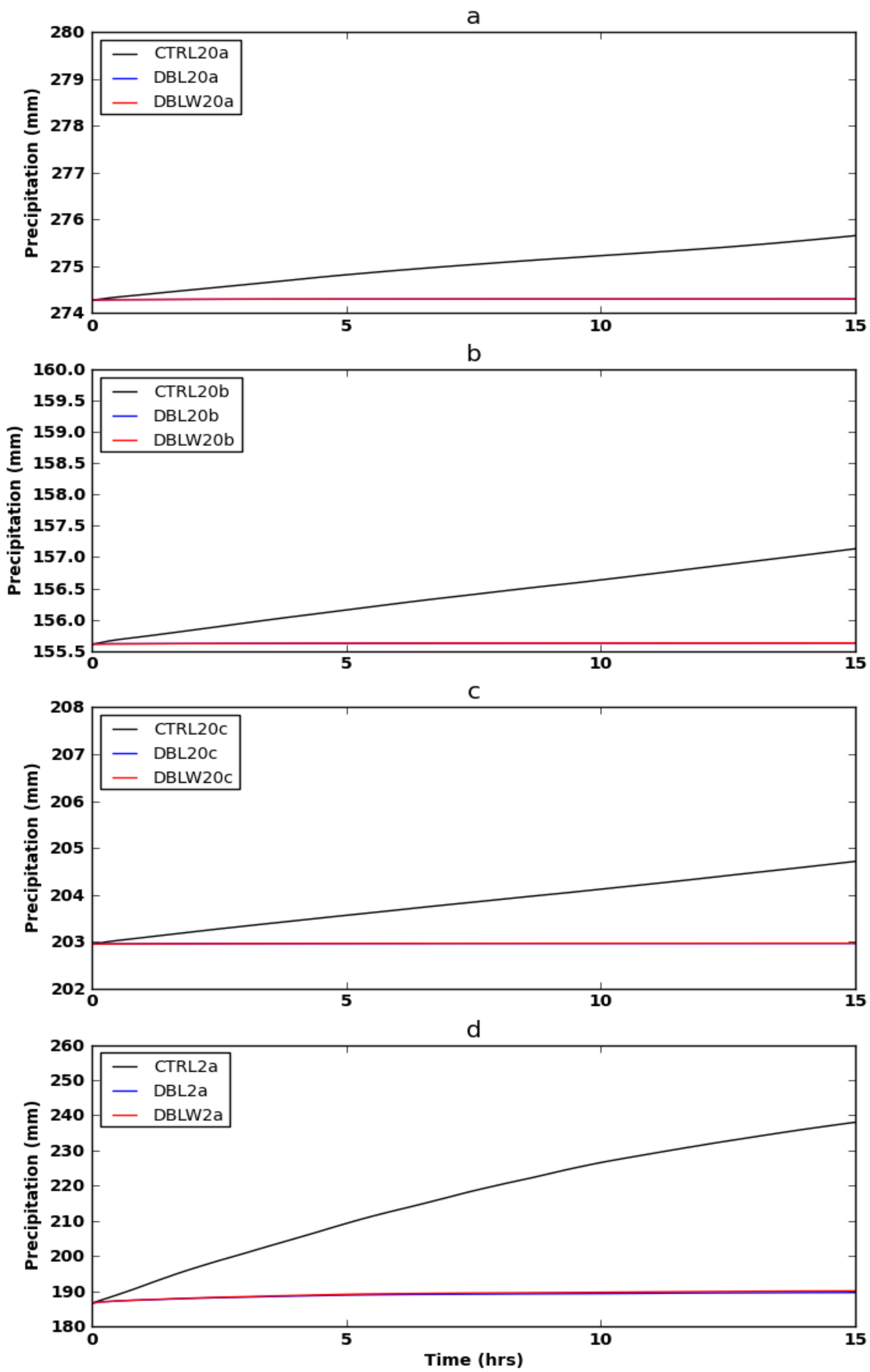

Supplementary Figure 10 Timeseries of domain averaged cumulative rainfall. Here black, red and blue line denotes CTRL, DBLW and DBL experiments respectively for the three sets of experiment a, b, c at 20 km resolution and one set of experiment a at 2 km resolution.

References and Notes

1. Betts, A. K., Miller, M. J. A new convective adjustment scheme. Part II: Single column tests using GATE wave, BOMEX, ATEX and arctic air-mass data sets. *Q. J. R. Meteorol. Soc.* **112**, 693–709 (1986).